Journal of Materials Chemistry A

Accepted Manuscript

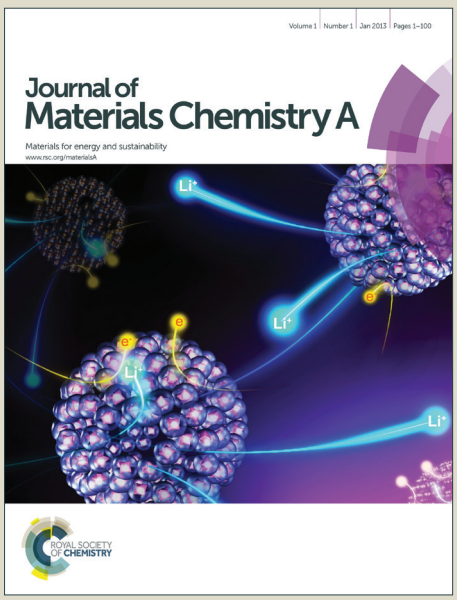

ROYAL SOCIETY OF CHEMISTRY

www.rsc.org/materialsA

Journal Name

RSCPublishing

ARTICLE

The Effect of Electronic Structure Changes in $NaInO_2$ and $NaIn_{0.9}Fe_{0.1}O_2$ on the Photoreduction of Methylene Blue

Cite this: DOI: 10.1039/x0xx00000x

Received ooth January 2012,
Accepted ooth January 2012

DOI: 10.1039/x0xx00000x

www.rsc.org/

Jonathan W. Lekse,[*ab] Barry J. Haycock,[ac] James P. Lewis,[ac] Douglas R. Kauffman[a] and Christopher Matranga[a]

Photochemical dye degradation is a promising method for organic pollutant remediation; however, this process has been limited by the efficiency of the catalyst materials with respect to photon absorption. An ideal catalyst would be capable of using as much of the solar spectrum as possible, in particular the visible region. One interesting class of materials that have the potential to provide this photoactivity is known as delafossites. These materials have the general formula ABO2 and are based on the mineral CuFeO2, also known as delafossite. They are especially interesting due to the ability to alter the band structure of these materials using chemical substitution. In particular, substitution on the B-site in these materials can be used to tune the physical properties of delafossites for specific applications. In this work, NaInO2 and NaIno.9Feo.1O2 have been studied and Fe substitution was found to decrease the band gap energy from 3.9 eV to 2.8 eV. The catalytic activity, measured by methylene blue dye degradation, of these delafossite materials was analysed and the reduction in band gap energy was found to result in increased visible light photoactivity. Computationally, thousands of supercells were examined in order to determine the most energetically favourable substituted structures and generate density of states plots in order to determine that the experimentally observed results were due to Fe-states increasing the energy of the highest occupied molecular orbitals.

Introduction

Organic pollutants such as textile dyes present an ecological hazard as they are frequently disposed of by dumping them into the nearest water supply.[1] These pollutants are harmful to species ranging from microorganisms to fish and even humans.[2] In order to reduce pollution, these compounds need to be removed from water using techniques such as carbon sorbents, ultrafiltration, reverse osmosis, and flocculation.[3-5] Removal options tend to be expensive and a more cost-effective alternative is desirable. Photocatalytic degradation provides a promising alternative for removal of these toxic compounds particularly if the catalyst can utilize a significant portion of the solar radiation reaching the Earth's surface.[6]

Some of the most promising catalyst materials for dye degradation employ the photo-Fenton process which involves the release of metal cations such as Fe^{2+} and Co^{2+} into solution.[7-9] Though effective at removing the organic dye molecules, the homogeneous nature of ions in solution makes recovery of the catalyst difficult and potentially cost-prohibitive, therefore a bulk photocatalyst would be preferred. Previous studies with photocatalytic dye degradation by solid materials have focused on oxides, particularly TiO_2, although other materials have also been tested.[1, 6, 10] The primary problem with oxides as photocatalysts is that they generally have wide band gaps and can only be photoexcited by ultraviolet light which only makes up 4-5% of the light reaching the earth's surface.[11, 12] As such, it is therefore prudent to investigate other oxide materials, particularly if the optical activity of these materials can be manipulated in a systematic fashion to utilize larger portions of the solar spectrum.

One particularly interesting class of bulk oxide materials with tunable electronic structures are the delafossite oxides with the general formula ABO_2 and a structure based on the mineral delafossite ($CuFeO_2$), Figure 1. Much of the previous research with delafossites has focused on thin film applications in transparent conducting oxides. However, these materials also show promise for photocatalytic applications due to their stability and interesting electronic structures. Substitution on the B-site in these materials alters the band structure resulting in a dramatic decrease in optical gap energy.[13-15] The reduction in gap energy is, in large part, due to the breaking of crystallographic inversion symmetry which changes the parity

of states close to the band edges and allows what were previously symmetry forbidden optical transitions to occur. This process of chemically breaking symmetry should enable the tuning of the electronic structure of delafossites and utilization of larger portions of the naturally available solar spectrum for photocatalytic applications. It is a particularly interesting approach for tuning the photocatalytic activity of $NaInO_2$, which has already demonstrated potential for decomposing organic pollutants[16, 17] as well as water splitting.[18] While the electronic structure of $NaInO_2$ has been previously studied in comparison to other related compounds such as $LiInO_2$[19] and $NaInS_2$,[20] substitution into the $NaInO_2$ structure

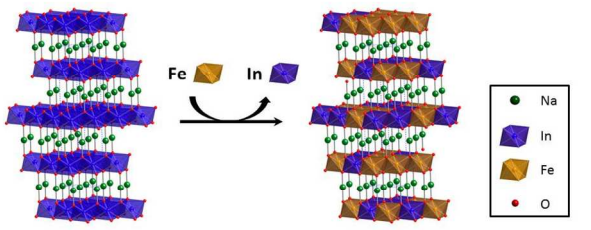

Figure 1. Rhombohedral crystal structure of the $NaInO_2$ and $NaIn_{0.9}Fe_{0.1}O_2$.

and the subsequent effect on electronic structure and photoactivity have not been thoroughly investigated. In this work, we investigate the effects of Fe-substitution on the electronic structure of $NaInO_2$ and how these changes alter the photocatalytic properties with respect to the decomposition of methylene blue.

Experimental Methods

Reagents and Synthesis of $NaInO_2$ and $NaIn_{1-x}Fe_xO_2$

The chemicals in this work were used as obtained: (i) Sodium Carbonate, Anhydrous, 99.5%, Alfa Aesar; (ii) Indium Oxide, 99.9%, Alfa Aesar, and (iii) Iron(III) Oxide, 99+%, Aldrich. $NaInO_2$ and $NaIn_{1-x}Fe_xO_2$ were synthesized from stoichiometric mixtures of Na_2CO_3, In_2O_3 and Fe_2O_3. The reaction mixtures were ground under acetone for 15 minutes, then the acetone was evaporated, the mixtures collected, and pressed into pellets. The pellets were heated in a box furnace from room temperature to 1100 °C in 24 hours, held at 1100 °C for 48 hours and then cooled to room temperature over 6 hours. Correct stoichiometry of the $NaInO_2$ and $NaIn_{1-x}Fe_xO_2$ final products was assured based on the ratio of the starting materials coupled with the lack of impurities observed in the powder diffraction patterns.

Physical Property Measurements

A Panalytical X'Pert Pro diffractometer was used to collect powder diffraction patterns for each sample. Scans were performed from 5 to 90 degrees 2-theta with a step size of 0.17 º and a scan speed of 200 s/º. HighScore Plus was used to perform Rietveld refinement on the collected patterns, in order to obtain unit cell dimensions of the substituted and unsubstituted compounds. A Perkin-Elmer Lambda 1050 dual-beam spectrometer was used to collect diffuse reflectance data for each compound from 200 to 2500 nm. The Kubelka-Munk equation[21] was then used to convert reflectance data into absorbance data for analysis. The value of the band gap was then determined using a standard method in which the absorption edge is extrapolated to zero. Electrochemical impedance spectroscopy was conducted in N_2 purged 0.5 M KCl using a Biologic SP150 electrochemical analyzer. Photocatalyst materials were bound to a glassy carbon working electrode using conductive carbon cement (SPI Supplies), and a Pt-wire counter electrode and Ag/AgCl reference electrode completed the cell. The Ag/AgCl reference electrode was calibrated against a Hydroflex reversible hydrogen electrode (RHE) and all potentials are reported in the RHE scale. Flatband potentials were extracted from Mott-Schottky plots of $1/C^2$ *vs.* electrode potential (Figure S1).

Catalysis Testing

Dye experiments were performed using a 20 μmol/mL solution of methylene blue dye. For each experiment, 0.1-0.15 g of catalyst was placed into a 20 mL beaker. 15.0 mL of dye solution was then added and allowed to equilibrate overnight for 12 hours in the dark. A Newport 300 W Xe arc lamp fitted with a manual shutter and an optical filter holder was used as the light source. Optical longpass filters were employed to remove high-energy portions of the lamp output in order to investigate visible light activity. The samples were stirred during reaction. Before spectroscopic analysis, the solution was centrifuged. 3 mL of the centrifuged solution was then placed into a quartz cuvette using a micropipette. The absorbance of the solution was then measured using an Agilent UV/Vis spectrometer. The spectrometer was blanked with 18 MΩ water before spectra were collected from 400-800 nm. In order to determine the iron ion concentrations in solutions, the dye solutions and controls were centrifuged and decanted into sample vials. These sample solutions were then analysed with an ICP-OES.

Computational Methods

For the computational work, we use density functional theory based on the local orbital method as implemented in the FIREBALL package[22]. The method allows for highly efficient DFT calculations of large supercells due to pre-computation of matrix elements before calculations are invoked. As a result, we conducted several thousand calculations simultaneously in order to find the optimal Fe configurations within the supercell and therefore the ones that most closely approximate the experimental systems. We use a single-numerical basis set within the local density approximation (LDA), with cutoffs (r_c) of O (r_c^s = 3.4 a_B, r_c^p = 3.8 a_B) and Na (r_c^s = 6.2 a_B, r_c^p = 6.7 a_B) with a single-numerical basis set with p- polarization for Fe (r_c^s = 5.3 a_B, r_c^p = 5.8 a_B, r_c^d = 4.7 a_B) and In (r_c^s = 5.1 a_B, r_c^p = 6.0 a_B, r_c^d = 4.7 a_B). The McWEDA functional for evaluating the

multi-center exchange-correlation interactions used throughout this work have proven to be effective for other oxide materials.[22-28]

We benchmark the chosen cutoffs against currently available experimental values for the lattice parameters of $NaInO_2$.[29] In the calculated supercells, a $NaInO_2$ primitive cell is used as the starting structure. $NaInO_2$ delafossite energetically favours the rhombohedral structure (space group no. 166, R3m), which contains four atoms in the unit cell. All atoms in the unit cell lie along the diagonal of the primitive cell starting with Na at the origin, In at the center of the cell, and O at 1/9 and 8/9 of the way along the diagonal of the cell. Our approach yields optimized lattice parameters that are within 3% of the experimentally reported parameters in the literature[29] of a = 3.235Å and c = 16.082Å for $NaInO_2$ and a = 3.022Å, c = 16.390Å for $NaFeO_2$.[29, 30]

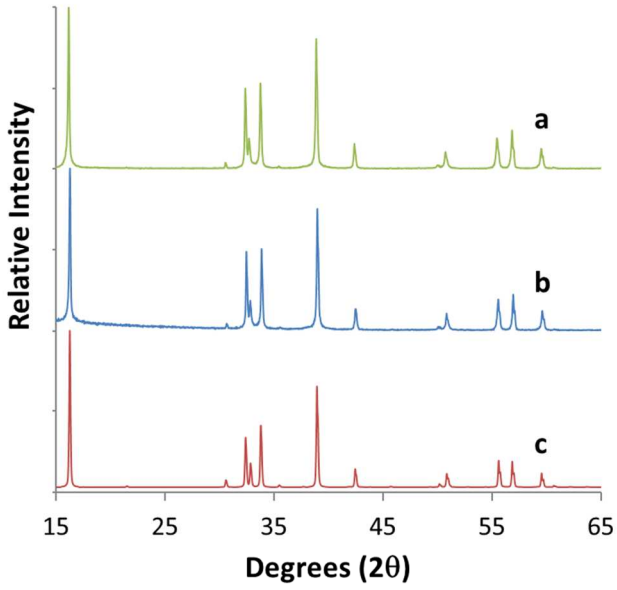

Figure 2. X-ray powder diffraction of a) $NaIn_{0.9}Fe_{0.1}O_2$, b) $NaInO_2$, and c) a reference pattern calculated for $NaInO_2$ from single crystal data.

Post-benchmarking, we generate a number of supercells based on the calculated lattice parameters. A 6x6x1 cell is chosen in the hexagonal coordinate system because it yields a 432 atom supercell, which therefore includes 108 possible substitution sites. The lattice vectors are scaled slightly with the amount of Fe substitution via Vegards' Law.[31] We calculate one supercell with no substituted atoms (i.e. the x = 0.0 case). For the x = 0.10 supercells, we apply a random site selection method used to choose where In is replaced with Fe in the supercells and carry out ~1000 calculations. After calculations are completed we choose the 10 lowest energy (and therefore the supercells with most likely Fe configurations) and calculate the electronic properties of the system. In this way we can accurately estimate what representative disordered structures would look like when obtained experimentally.

Results and Discussion

Previous work with related delafossite systems has indicated that substitution on the B-site will result in symmetry breaking which can lead to increased optical properties.[13-15] Likewise, substitution on the B-site in $NaInO_2$ will potentially result in improved catalytic performance. Fe was selected for substitution for several reasons including its formation of the rhombohedral delafossite $NaFeO_2$ that is isostructural to $NaInO_2$ which prevents phase segregation during B-site alloying; our previous success in using it for B-site alloying with the $CuGaO_2$ system; and its relatively benign environmental impacts.[13] In order to test our hypothesis, $NaInO_2$ and $NaIn_{0.9}Fe_{0.1}O_2$ samples were prepared by a traditional solid state reaction based on previous literature preparations,[32] with no additional requirements needed to obtain the Fe-substituted sample. Both Fe and In delafossites favour the rhombohedral structure which allows for the synthesis of a solid solution instead of phase segregation. As expected, the compounds crystallized in a rhombohedral delafossite structure, Figure 1. Unlike the synthesis of related copper delafossites, the preparation of sodium delafossites can be performed in air, primarily due to the preference of sodium for the 1^+ oxidation state compared to copper which disproportionates into a mixture of copper metal, Cu^0, and Cu^{2+} upon heating in air. X-ray powder diffraction was used to determine the phase purity of the obtained samples. The powder patterns for substituted and unsubstituted samples were nearly identical, Figure 2. Subtle, systematic differences were observed in peak position, due to changes in the unit cell volume as a result of iron incorporation.

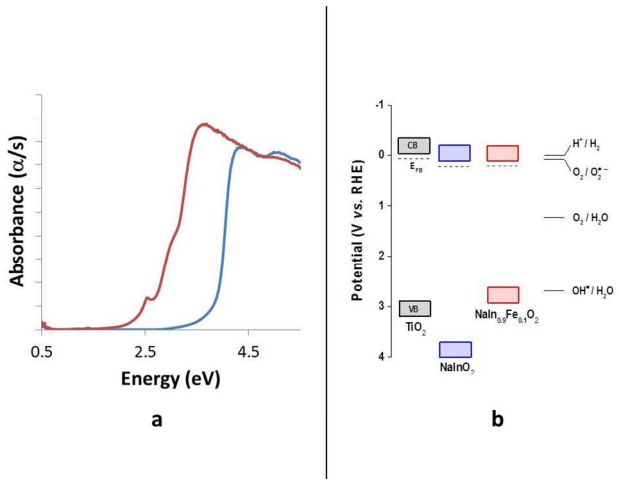

Figure 3. Diffuse reflectance spectroscopy was used to determine the band gap values of 3.9 eV and 2.8 eV for $NaInO_2$ and $NaIn_{0.9}Fe_{0.1}O_2$, respectively (a). Energy level diagram describing the flatband (E_{FB}; dashed line), conduction band (E_{CB}) and valence band (E_{VB}) potentials of TiO_2, $NaInO_2$ and $NaIn_{0.9}Fe_{0.1}O_2$ in relation to some relevant electrochemical redox couples; potentials are in the reversible hydrogen electrode (RHE) scale (b). The spread in CB and VB potentials represents the experimental uncertainty in band edge determination.

Visual analysis of the samples following reaction showed a distinct qualitative difference in the color of the Fe-containing samples which were yellow in comparison to the unsubstituted samples which were white. This color change is evidence of changes in the electronic structure due to iron incorporation. We employed diffuse reflectance spectroscopy in order to quantify these changes, to estimate the band gap energy of the samples, and to gain additional understanding of the effect of Fe-substitution, Figure 3a. $NaInO_2$ was found to have a band gap of 3.9 eV. Fe substitution was found to reduce the band gap energy in $NaIn_{0.9}Fe_{0.1}O_2$ to 2.8 eV, a change of over 1 eV. A decrease in band gap energy was expected and mirrors similar changes observed when Fe was substituted into $CuGaO_2$.[13] These experimental and computational results reinforced the hypothesis previously advanced by Huda, *et. al* that the symmetry forbidden fundamental gap could be accessed by B-site substitution.[14, 15] In our study of the $NaIn_{1-x}Fe_xO_2$ system, the experimentally observed decrease in band gap energy is computationally linked to a combination of factors discussed in more detail below including an increase in the Fermi level, Figure 4, and stress within the crystalline lattice, Figure 5.

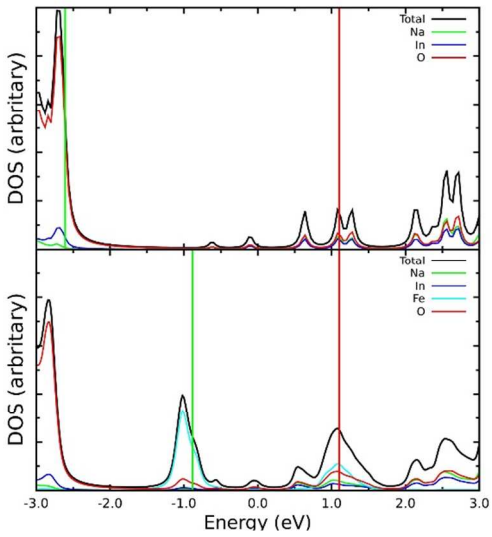

Figure 4. Density of states (DOS) plots for (top) $NaInO_2$ and (bottom) $NaIn_{0.9}Fe_{0.1}O_2$. The introduction of Fe creates filled states within the gap, raising the energy of the highest occupied molecular orbital (HOMO) and increasing the number of states at the valence band edge. The green vertical line represents the valence band edge (HOMO), or the Fermi energy. The red line represents the conduction band edge.

Electrochemical impedance spectroscopy was used to construct Mott-Schottky plots for flatband potential (E_{FB}) determination (Figure S1).[33, 34] TiO_2, $NaIn_{0.9}Fe_{0.1}O_2$ and $NaInO_2$ showed characteristic n-type behavior with E_{FB} values of 0.066±0.019 V, 0.213±0.025 V and 0.223±0.016 V *vs.* the reversible hydrogen electrode (RHE), respectively; standard deviations represent triplicate measurements. $NaIn_{0.9}Fe_{0.1}O_2$ and $NaInO_2$ showed statistically equivalent E_{FB}, and the TiO_2 E_{FB} is consistent with other literature reports.[35, 36] The conduction band potential (E_{CB}) of n-type metal oxides is approximately −0.1V to −0.4V more negative (higher energy) than the measured E_{FB}, which provides upper and lower bounds for the CB edge.[37] The valence band (VB) is located at more positive potentials (lower energy) compared with the CB, and the valence band potential (E_{VB}) can be estimated relative to E_{CB} from the material's optical bandgap ($E_{VB} = E_{CB} + E_g$).[37] Figure 3b presents an energy level diagram containing the photocatalysts' E_{FB}, E_{CB} and E_{FB} in relation to relevant electrochemical redox couples.[38] The range in the CB and VB position reflects the experimental uncertainty in band edge determination; however, the estimated CB and VB potentials are consistent with the potentials required to form the $O_2^{\bullet-}$ (0.083 V *vs.* RHE) and $OH^{\bullet}$ (2.7 V *vs.* RHE) radicals identified in the MB degradation mechanism (discussed below).[38]

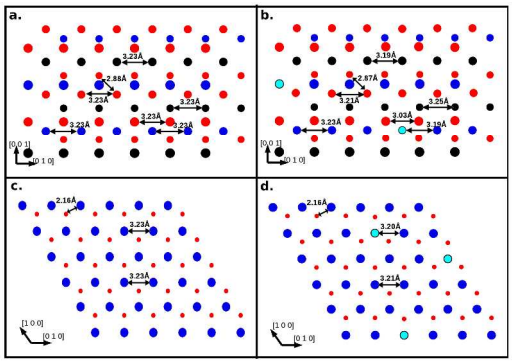

Figure 5. Example of crystal changes due to the introduction of Fe for In. Solid red circles represent O, solid black circles are Na, cyan circles with a black border represent Fe atoms and solid blue circles represent In atoms. These images are directly plotted from calculated supercells, cleaved in the planes corresponding to the image axis. We have scaled the circles in **a.** and **b.** with respect to their relative out-of-plane distances, showing the O atoms that are further forward than the Na and In planes. Measurements shown are directly from calculated supercells, and representative of the 1000+ supercells calculated for this study.

Figure 4 shows the calculated PDOS of the undoped cell and the average of the 10 most energetically favorable supercells in the $NaIn_{0.90}Fe_{0.10}O_2$ study. The electronic calculations of the undoped structure yield an electronic gap between the highest occupied molecular orbital (HOMO) and the lowest unoccupied molecular orbital (LUMO) of ~2.0eV. However, upon inspection of the wavefunction localization, which correspond to the nature of the dipole transitions,[39] we find that the optical gap actually extends well above the conduction band edge (to the red line in Figure 4) and the calculated optical gap is ~3.8eV. Of our 1000 calculated $NaIn_{0.90}Fe_{0.10}O_2$ supercells, the most energetically favourable structures yield broadening in the optical conduction band edge (red line in Figure 4). The reduction of the optical gap is solely dependent on the increase in the valence band edge causing a significant shift in the Fermi energy. Examination of the partial density of states (PDOS) plots in Figure 4 shows that new states arise in the Fe-doped system and are solely due to electronic contributions from Fe-sites, leading to the lower band gap observed experimentally. Based on Figure 4 the experimental

band gap observed in Figure 3 for $NaIn_{0.9}Fe_{0.1}O_2$ is most likely due to transitions between the new Fe valence edge (HOMO) states and the Fe-O states ~2eV above. The Fe based filled bands have the effect of raising the Fermi energy by about 1.5eV, which is the major cause of the closing of the gap. Our calculations show that these new Fe states are highly localized in general, with a single hybrid Fe and O based state that is very dispersed at the valence band edge. The conduction band energy does not change as a result of Fe substitution which is consistent with the results of the flatband potential measurements, Figure 3b.

In the crystallographic calculation, we find that the Fe sites cause an overall strain on the crystal due to their comparatively smaller volume than the In. The Fe – In, Fe – O and Fe – Na bonds are shorter than the In – In, In – O and In – Na bonds leading not only to a global strain on the entire crystal structure but also to localized strain on the bonds about the Fe filled sites. In the undoped structure we measure an average In – Na bond distance of 3.266Å, with a statistical variance of $2.4x10^{-3}$Å. In our previous computational study of $CuGa_{1-x}Fe_xO_2$, a reduction in supercell energy was correlated with a reduction in the A-site to B-site bond length statistical variance.[13, 40] There was no reduction in the statistical variance with energy in the $NaIn_{0.9}Fe_{0.1}O_2$ supercells. In all $NaIn_{0.9}Fe_{0.1}O_2$ supercells calculated, the equivalent measurement (that is, In site containing either Fe or In to first nearest neighbor Na) is ~2.642Å with a statistical variance of $\sim1.7x10^{-2}$Å. Similarly, in the undoped structure, we measure In-In nearest neighbor distances of between 3.234Å and 3.236Å after relaxation of the supercell and Na – Na distances of between 3.234Å and 3.236Å. In the $NaIn_{0.9}Fe_{0.1}O_2$ supercells, these measurements vary greatly, we find that the Fe to first nearest neighbor In varies from ~3.16Å to ~3.19Å, and the average In – In bond length is ~3.21Å. Near an Fe site the In – In bonds are under local strain, we measure these bonds as ~3.24Å. Overall, the presence of Fe atoms in the $NaInO_2$ supercells significantly modifies the entire crystal lattice and introduces irregularities in the material. Figure 5 depicts an example of the introduced short and long-range disorder due to the presence of Fe.

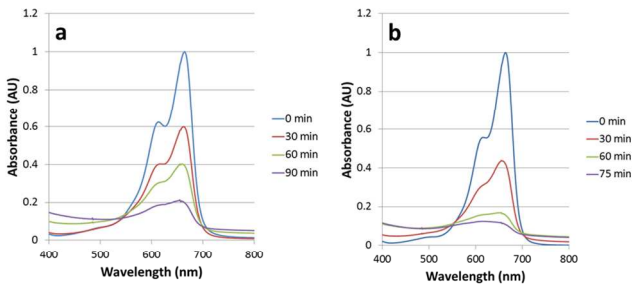

Figure 6. UV/Vis spectroscopy of the decomposition of methylene blue dye by a) $NaIn_{0.9}Fe_{0.1}O_2$ and b) $NaInO_2$. $NaInO_2$ is more active than $NaIn_{0.9}Fe_{0.1}O_2$ with broadband light.

The changes in the electronic structure of the substituted sample noted above should also result in an improvement of the photocatalytic activity of the $NaIn_{0.9}Fe_{0.1}O_2$ system in comparison to the unsubstituted sample. To probe how these electronic structure changes impact catalytic activity, we have used the photodegradation of Methylene Blue (MBu) dye as a model reaction to mimic the remediation of aqueous organic pollutants.[16, 17] In previous work, the $NaInO_2$ samples were sensitized with a variety of co-catalysts such as NiO, RuO_2, and Pt.[16] These co-catalysts were found to improve the decomposition of the dye. However, in order to simplify the system and gain a more complete understanding of how the physicochemical properties change as a result of alterations in the electronic structure due to iron substitution, we did not utilize co-catalysts. The initial experiments with $NaInO_2$ and $NaIn_{0.9}Fe_{0.1}O_2$ were performed using broadband light from a Xe arc lamp. Both samples were found to decompose MBu as evidenced by a loss of the blue color in the solution which was monitored using UV-Vis spectroscopy, Figure 6. The reaction was found to follow pseudo first order kinetics which is consistent with previous work that details a radical mediated mechanism, Figure 7.[1, 41-43] In previous studies with other photocatalyst systems, addition of an oxidizer such as H_2O_2 was required for dye decomposition;[7] however, additional oxidizers were not required for enhancing the activity of these delafossite materials. Under broadband light, the unsubstituted sample performs slightly better than the substituted delafossite, requiring approximately 75 minutes for nearly complete decomposition of the dye as opposed to longer than 90 minutes for the substituted sample.

While iron substitution does not increase the photoactivity of the delafossite under broadband light, the smaller band gap energy does enable the use of visible light only for photodecomposition. To illustrate this, long-pass filters were used to progressively eliminate the higher energy UV portions of the broadband lamp spectrum leaving only longer visible and near-infrared wavelengths for photoexcitation of the sample. Dye decomposition was found to continue with the $NaInO_2$ sample when the 295 nm (4.20 eV) filter was used but addition of the 305 nm (4.06 eV) filter resulted in no observable decomposition of the MBu, Figure 6. The 305 nm filter is close to the experimentally determined band gap energy of approximately 318 nm and indicates the lack of photocatalytic activity below these energies results from sub-gap excitation of the $NaInO_2$ and a lack of mobile carriers being promoted into the conduction band. In contrast, the Fe-substituted, $NaIn_{0.9}Fe_{0.1}O_2$ continued photodecomposition of the dye with the 305 nm (4.06 eV), 380 nm (3.26 eV), 405nm (3.06 eV) and 420 nm (2.95 eV) filters, well past the point at which the unsubstituted sample was found to cease activity, Figure 7.

The increased photoactivity observed in $NaIn_{0.9}Fe_{0.1}O_2$ compared to $NaInO_2$ is likely due to the decrease in the band gap energy noted experimentally, Figure 3, and computationally, Figure 4. The decrease in band-gap energy from 3.9 to 2.8 eV still allows for light at 420 nm (2.95 eV) and lower energies to photoexcite charge carries in the $NaIn_{0.9}Fe_{0.1}O_2$. The photoexcited electrons and holes must also have reasonable mobility and be capable of diffusing to the

physical edges of the catalyst particle where they can initiate redox processes. As such, our photocatalytic results indicate that Fe is substituted directly in place of In and the added Fe atoms do not act as significant scattering centers for the photoexcited electrons and holes. In the case of MBu degradation, this photoexcited electrons and holes migrate to the catalyst surface where they interact with water in the solution. The electrons are responsible for initiating the production of superoxide oxygen radicals ($O_2^{\cdot -}$) that in turn react with a proton to form $HO_2^{\cdot}$, while the holes react directly with water to produce $OH^{\cdot}$. These radicals, $O_2^{\cdot -}$, $OH^{\cdot}$, and $HO_2^{\cdot}$ then repeatedly degrade the dye molecule to simple compounds such as CO_2 and H_2O.[1, 41-43] Our filter set studies also show a brief induction period followed by decomposition that follows pseudo first order kinetics similar to the process under broadband light. We attribute this induction period to time required to produce a large enough radical population to decompose the dye.

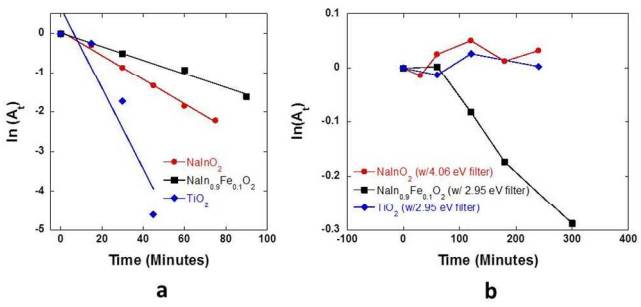

Figure 7. Absorbance data illustrating the decomposition of methylene blue as a function of time with broadband light (a) and with the use of different band pass filters (b). Plotting $\ln(A_t)$ demonstrates that the decomposition follows pseudo first order kinetics.

As a control experiment, we wanted to rule out the possibility that the increased efficiency of $NaIn_{0.9}Fe_{0.1}O_2$ was due to the photoinduced release of iron cations into solution resulting in a homogeneous catalysis process similar to what has been previously observed with Co^{2+} ions.[8, 9] For this control run, a series of dye degradation experiments were run with either $NaInO_2$ or $NaIn_{0.9}Fe_{0.1}O_2$ and the reaction solutions were tested for the presence of iron both before and after the light-induced catalytic reaction. The dye solution with $NaInO_2$ was found to contain no iron cations after light exposure, while the solution with the $NaIn_{0.9}Fe_{0.1}O_2$ catalyst following reaction was found to contain ~70 μg/L iron. While this concentration is small, the potential for the Fe^{3+} to contribute to the catalytic activity is present and had to be further eliminated. To this end, a second control experiment with a solution of $Fe(NO_3)_3$ with a concentration of 700 μg Fe/L and the 320 nm (3.87 eV) filter was conducted. No dye decomposition was observed despite a concentration 100x that of the concentration of Fe cations in the delafossite experiment. This result implies that the increased photodecomposition activity observed with the $NaIn_{0.9}Fe_{0.1}O_2$ catalyst was due to the changes in the electronic structure of the substituted delafossite not from any Fe^{3+} ions leached into solution during the photoreaction.

In addition to the two delafossite samples, we also tested a nanoparticulate TiO_2, commercially known as P25, as a benchmark for the photoactivity experiments, Figure 7. Under broadband illumination, the decomposition of MBu dye by the delafossite materials is significantly slower than the decomposition by TiO_2, which completely decomposed the dye in 45 minutes compared to 75 and 90 minutes for unsubstituted and substituted delafossites respectively. The photoactivity of the TiO_2 was significantly reduced when the long pass filters were added and UV light removed from the excitation light source. Under these conditions, the TiO_2 and $NaIn_{0.9}Fe_{0.1}O_2$ had comparable rates of dye decomposition. Photoactivity of the TiO_2 system ceased when the 420 nm (2.95 eV) filter was used while $NaIn_{0.9}Fe_{0.1}O_2$ continued to degrade the dye until the 475 nm (2.61 eV) filter was added. Based on band gap energies, this result is expected as the measured band gap for $NaIn_{0.9}Fe_{0.1}O_2$ is 2.8 eV compared to >3.2 eV for P25.

Conclusions

In conclusion, we synthesized iron substituted $NaIn_{0.9}Fe_{0.1}O_2$ was synthesized for the first time and its catalytic activity for the decomposition of methylene blue dye compared to the unsubstituted $NaInO_2$. Under broadband light exposure, both substituted and unsubstituted samples were found to photodecompose methylene blue dye, though not as efficiently as nanoparticulate TiO_2. As the high energy light was removed with longpass filters, $NaIn_{0.9}Fe_{0.1}O_2$ exhibited greater photoactivity than $NaInO_2$ and eventually TiO_2. The increase in photoactivity can be traced to B-site substitution into the delafossite structure causing electronic structure changes. These changes have been successfully modelled computationally and show that B-site substitution results in a decrease in the band gap energy due to filled states of higher energy than the undoped material due to the Fe atoms and a change in orbital configuration that is indicative of symmetry breaking in the crystal. This combination of experimental and computational results in this work represents a significant step towards the design and synthesis of new more efficient photocatalysts.

Acknowledgements

As part of the National Energy Technology Laboratory's Regional University Alliance (NETL-RUA), a collaborative initiative of the NETL, this technical effort was performed under the RES contract DE-FE0004000. This work was also supported, in part, by the National Science Foundation through NSF DMR 09-03225. This report was prepared as an account of work sponsored by an agency of the United States Government. Neither the United States Government nor any agency thereof, nor any of their employees, makes any warranty, express or implied, or assumes any legal liability or responsibility for the

Notes and references

[*]Tel:1-412-386-7312;E-mail:
Jonathan.Lekse@CONTR.NETL.DOE.GOV
[a] National Energy Technology Laboratory, United States Department of Energy, Pittsburgh, PA 15236, USA.
[b] URS, South Park, PA 15129, USA.
[c] Department of Physics, West Virginia University, Morgantown, West Virginia 26506-6315, USA.

Electronic Supplementary Information (ESI) available: Additional information regarding the electrochemical impedance spectroscopy experiments and additional dye decomposition absorbance data. See DOI: 10.1039/b000000x/

1. S. H. S. Chan, T. Y. Wu, J. C. Juan and C. Y. Teh, *J. Chem. Technol. Biotechnol.*, 2011, **86**, 1130-1158.
2. Z. M. El-Bahy, A. A. Ismail and R. M. Mohamed, *J. Hazard. Mater.*, 2009, **166**, 138-143.
3. A. N. Rao, B. Sivasankar and V. Sadasivam, *J. Mol. Catal. A-Chem.*, 2009, **306**, 77-81.
4. M. A. Rauf and S. S. Ashraf, *J. Hazard. Mater.*, 2009, **166**, 6-16.
5. Z. S. Seddigi, *Bull. Environ. Contam. Toxicol.*, 2010, **84**, 564-567.
6. A. Mills and S. LeHunte, *J. Photochem. Photobiol. A-Chem.*, 1997, **108**, 1-35.
7. J. Herney-Ramirez, M. A. Vicente and L. M. Madeira, *Appl. Catal. B-Environ.*, 2010, **98**, 10-26.
8. N. N. Binitha, P. V. Suraja, Z. Yaakob, M. R. Resmi and P. P. Silija, *J. Sol-Gel Sci. Technol.*, 2010, **53**, 466-469.
9. S. K. Ling, S. B. Wang and Y. L. Peng, *J. Hazard. Mater.*, 2010, **178**, 385-389.
10. A. Mills and J. S. Wang, *J. Photochem. Photobiol. A-Chem.*, 1999, **127**, 123-134.
11. S. J. Zhang and L. M. Song, *Catal. Commun.*, 2009, **10**, 1725-1729.
12. Y. Y. Lv, L. S. Yu, H. Y. Huang, H. L. Liu and Y. Y. Feng, *J. Alloy. Compd.*, 2009, **488**, 314-319.
13. J. W. Lekse, M. K. Underwood, J. P. Lewis and C. Matranga, *J. Phys. Chem. C*, 2012, **116**, 1865-1872.
14. M. N. Huda, Y. F. Yan, A. Walsh, S. H. Wei and M. M. Al-Jassim, *Appl. Phys. Lett.*, 2009, **94**.
15. M. N. Huda, Y. F. Yan, A. Walsh, S. H. Wei and M. M. Al-Jassim, *Phys. Rev. B*, 2009, **80**.
16. J. H. Wang and T. Nonami, *Journal of Materials Science*, 2004, **39**, 6367-6370.
17. J. H. Wang and T. Nonami, in *Science of Engineering Ceramics Iii*, eds. T. Ohji, T. Sekino and K. Niihara, Trans Tech Publications Ltd, Zurich-Uetikon, 2006, pp. 819-822.
18. J. Sato, H. Kobayashi, N. Saito, H. Nishiyama and Y. Inoue, *J. Photochem. Photobiol. A-Chem.*, 2003, **158**, 139-144.
19. S. Kawakami, M. Sasaki, H. Tabata, H. Shimooka, S. Kohiki, S. Matsushima, M. Oku and T. Shishido, *J. Alloy. Compd.*, 2003, **359**, 278-280.
20. S. Matsushima and S. Kohiki, *Chemistry Letters*, 2000, 8-9.
21. P. Kubelka and F. Munk, *Z Tech Phys*, 1931, **12**, 593-601.
22. J. P. Lewis, P. Jelínek, J. Ortega, A. A. Demkov, D. G. Trabada, B. Haycock, H. Wang, G. Adams, J. K. Tomfohr, E. Abad, H. Wang and D. A. Drabold, *Phys. Stat. Sol. (b)*, 2011, 1-19.
23. P. Jelinek, H. Wang, J. P. Lewis, O. F. Sankey and J. Ortega, *Phys. Rev. B*, 2005, **71**, 235101.
24. R. Asahi, T. Morikawa, T. Ohwaki, K. Aoki and Y. Taga, *Science*, 2001, **293**, 269-271.
25. B. Prasai, B. Cai, D. A. Drabold, M. K. Underwood and J. P. Lewis, *MS&T-11 Conf. Proceedings* 2011.
26. H. Wang and J. P. Lewis, *J. Phys. Condens. Matter*, 2005, **17**, L209-L213.
27. H. Wang and J. P. Lewis, *J. Phys. Condens. Matter*, 2006, **18**, 421-434.
28. H. Wang and J. P. Lewis, *Physica Status Solidi B-Basic Solid State Physics*, 2011, **248**, 2037-2043.
29. K. Fukuzaki, S. Kohiki, S. Matsushima, M. Oku, T. Hideshima, T. Watanabe, S. Takahashi and H. Shimooka, *Journal of Materials Chemistry*, 2000, **10**, 779-782.
30. B. V. Beznosikov and K. S. Aleksandrov, *J Struct Chem+*, 2009, **50**, 102-107.
31. A. R. Denton and N. W. Ashcroft, *Physical Review A*, 1991, **43**, 3161-3164.
32. K. Fukuzaki, S. Kohiki, S. Matsushima, M. Oku, T. Hideshima, T. Watanabe, S. Takahashi and H. Shimooka, *Journal of Materials Chemistry*, 2000, **10**, 779-782.
33. A. W. Bott, *Current Separations*, 1998, **17**, 87-91.
34. K. Gelderman, L. Lee and S. W. Donne, *J. Chem. Ed.*, 2007, **84**, 685-688.
35. N. Baram and Y. Ein-Eli, *J. Phys. Chem. C*, 2010, **114**, 9781-9790.
36. R. Beranek, *Adv. Phys. Chem.*, 2011, **2011**, Article ID 786759.
37. B. A. Pinaud, Z. Chen, D. N. Abram and T. F. Jaramillo, *J. Phys. Chem. C*, 2011, **115**, 11830–11838.
38. P. Wardman, *J. Phys. Chem. Ref. Data*, 1989, **18**, 1637-1755.
39. J. P. Lewis, T. E. Cheatham, E. B. Starikov, H. Wang and O. F. Sankey, *J. Phys. Chem. B*, 2003, **107**, 2581-2587.
40. B. J. Haycock, M. Kylee Rice and J. P. Lewis, *Computational Materials Science*, 2014, **86**, 155-164.
41. D. Chatterjee and S. Dasgupta, *J. Photochem. Photobiol. C-Photochem. Rev.*, 2005, **6**, 186-205.
42. A. Houas, H. Lachheb, M. Ksibi, E. Elaloui, C. Guillard and J. M. Herrmann, *Appl. Catal. B-Environ.*, 2001, **31**, 145-157.
43. Q. Wang, S. L. Tian and P. Ning, *Ind. Eng. Chem. Res.*, 2014, **53**, 643-649.